

Design Analysis of OAM Fibers using Particle Swarm Optimization Algorithm

Jun Ho Chang, Alessandro Corsi, Leslie A. Rusch and Sophie LaRochelle

IEEE/OSA Journal of Lightwave Technology, (published 7 October 2019)

Doi: 10.1109/JLT.2019.2945870

<https://ieeexplore.ieee.org/document/8861154>

© 2019 IEEE. Personal use of this material is permitted. Permission from IEEE must be obtained for all other uses, in any current or future media, including reprinting/republishing this material for advertising or promotional purposes, creating new collective works, for resale or redistribution to servers or lists, or reuse of any copyrighted component of this work in other works.

Design Analysis of OAM Fibers using Particle Swarm Optimization Algorithm

Jun Ho Chang, Alessandro Corsi, Leslie A. Rusch, *Fellow, IEEE*, and Sophie LaRochelle, *Senior Member, IEEE*

Abstract—We study the design of ring core fibers (RCFs) supporting orbital angular momentum (OAM) modes for mode division multiplexing (MDM) transmission systems. We develop target criteria to optimize fiber designs using a particle swarm optimization (PSO) algorithm under fabrication constraints. Effective index separation, Δn_{eff} , and polarization purity of each OAM mode are known to determine modal crosstalk levels. To reduce the complexity of multiple-input multiple-output (MIMO) processing required to compensate for modal crosstalk, we define an objective function based on these quantities. Our design analysis focuses on four different concepts of step-index RCF leading to different modal and structural characteristics. The optimum design for each concept is derived using the PSO algorithm. We investigate the impact of hollow-core and/or higher-order radial modes on Δn_{eff} and polarization purity. Design strategies for increasing Δn_{eff} and polarization purity are discussed in light of robustness to fabrication errors. We finally discuss the scalability and potential limitations of this design.

Index Terms—Fiber design, mode division multiplexing (MDM), orbital angular momentum (OAM), ring core fiber (RCF), space division multiplexing (SDM), few mode fiber (FMF).

I. INTRODUCTION

MODE division multiplexing (MDM) has attracted considerable attention as a promising technology to meet the ever-increasing demand for fiber-optic network capacity [1]. A set of spatially orthogonal modes in a multi-mode fiber, each of which carries an independent optical signal, is exploited to boost the capacity beyond the nonlinear Shannon limit inherent to conventional single-mode fiber. Linearly polarized (LP) modes have typically been used as a modal basis for MDM because they are more readily excited and detected than true vector modes [1]. Thus, several MDM transmissions based on LP modes have been demonstrated over weakly-guiding multi-mode fibers [2]-[9].

During recent years, orbital angular momentum (OAM) modes have emerged as another orthogonal modal basis for MDM due to their attractive optical properties [10]-[15]. An OAM mode has a helical phase front characterized by the number of phase rotation over the field distribution plane, l ,

which is known as the topological charge. As opposed to LP modes that exist as a superposition of multiple degenerate vector modes, circularly-polarized OAM modes with a topological charge of $|l|$ are composed of only one vector mode, either $HE_{l+1,m}$ or $EH_{l-1,m}$ [16]. This provides an opportunity to simplify or eliminate complex multiple-input multiple-output (MIMO) processing, which is required in MDM systems using LP modes to exploit full modal basis. However, it should be noted that the polarization of OAM mode generally departs from perfect circular states due to spin-orbit coupling [17-18]. In conventional optical fiber, the OAM modes are known to be unstable and easily convert into LP modes because the $HE_{l+1,m}$ and $EH_{l-1,m}$ modes are nearly degenerate, which results in strong coupling during propagation [10]. Therefore, it is necessary to use fibers optimized to lift the modal degeneracies between these vector modes.

A ring core structure with high refractive index contrast can increase the effective index difference (Δn_{eff}) between $HE_{l+1,m}$ and $EH_{l-1,m}$ modes. In [19], various designs of step-index ring-core fibers (RCFs) were discussed to achieve Δn_{eff} of $\sim 10^{-4}$ for the OAM modes with $|l|=1$ and 2. RCFs with graded index [20], inverse parabolic index [21], photonic crystal structure [22], and trench-assisted index [23] have also been proposed to increase Δn_{eff} and thus mitigate mode coupling. In [24], an analytical study showed that the degeneracy can be strongly broken if abrupt refractive index change coincides with large field amplitude of transverse mode and its field gradient. In this context, hollow-core RCF (whose inner “cladding” of the ring-shaped core is air) has been regarded as one of the most promising designs because of the extremely high index contrast at the interface of its core and inner cladding. Various designs of hollow-core RCFs have been proposed [25-27] and some notable transmission experiments have been successfully demonstrated [28-29].

Despite the many RCF design concepts proposed so far, their optimization process is complex, not only due to time-consuming and tedious test-and-trial approaches, but also because the optimum design may vary in different circumstances, e.g., target number of modes, allowable crosstalk level, and structural constraints for fabrication.

Manuscript received xx, 2019; revised xx, 2019.

Date of publication xx ; date of current version xx. (*Corresponding author: Jun Ho Chang*)

This work was supported by Huawei Canada and NSERC (CRDPJ 515539-17). This work is part of the research program of the Canada Research Chair on Advanced Photonic Technologies for Communications.

J. H. Chang, A. Corsi, L. A. Rusch, and S. LaRochelle are with the Centre for Optics, Photonics and Lasers, Department of Electrical and Computer

Engineering, Université Laval, Québec, QC, G1V 0A6, Canada (e-mail: junho.chang.1@ulaval.ca; alessandro.corsi.1@ulaval.ca; leslie.rusch@gel.ulaval.ca; sophie.larochelle@gel.ulaval.ca).

Color versions of one or more of the figures in this paper are available online at <http://ieeexplore.ieee.org>.

Digital Object Identifier xxx

Therefore, it is beneficial to develop a systematic optimal fiber design using criteria derived from total system requirements. The particle swarm optimization (PSO) algorithm is a population-based solution-finding method that has been widely employed for solving various optimization problems [30]. Similar to other evolutionary search techniques such as the genetic algorithm, a swarm of potential solutions (i.e., particles) is randomly generated to initiate the PSO algorithm. At every iteration, based on its own experience and the swarm's experience, each particle updates its current position to achieve a better position in the search space. The particles remember the best position that each individual particle has experienced, as well as the best global position of the swarm. Compared to the genetic algorithm, PSO is known to be more computationally efficient for solving problems with continuous design variables [31]. For this reason, it has been utilized for optimizing bend-insensitive optical fiber [32], grating couplers [33], and fiber amplifiers [34].

In this paper, we propose a PSO algorithm to find the optimal RCF design, taking into account various physical features important for MDM transmission systems. These features include the number of usable OAM modes, the minimum Δn_{eff} , bending loss, and modal purity, and all these properties are considered in the objective score of a design. To confirm the utility of this method, we optimize step-index RCFs for various design criteria, and discuss their modal characteristics and suitability for MDM systems. We discuss the relative merits of the different design strategies. We also investigate the impact of variations of geometric parameters on the objective score. Although we focus only on the RCF designs aiming for vector mode multiplexing (i.e., in which $HE_{l+1,m}$ and $EH_{l-1,m}$ are regarded as two uncoupled modes), our optimization process can also be applied to fibers targeting mode group multiplexing (i.e., in which $HE_{l+1,m}$ and $EH_{l-1,m}$ are likely to couple to each other), which generally requires less stringent design constraints.

The remaining sections of this paper are organized as follows. In Section II, we discuss the fiber design criteria for OAM MDM transmission. In Section III, we describe the PSO algorithm for finding the optimal geometric parameters. In Section IV, the designs optimized for three OAM mode groups are derived, and the impact on modal characteristics of a hollow-core and/or the presence of higher-order radial modes is discussed. In Section V, we present the results for the design with a higher number of OAM modes. The tolerance analysis and the design strategy are covered in Section VI. Finally, we conclude the paper in Section VII.

II. RING-CORE FIBER FOR OAM MDM TRANSMISSION

Consider the $OAM_{|l|,m}$ mode with right or left circular polarization (RCP or LCP), where l is the topological charge and m is the number of concentric rings in the intensity profile of the mode. It can be expressed solely in terms of $HE_{l+1,m}$ or $EH_{l-1,m}$, which of the two depends on the polarization state as explained below. For $|l| > 1$, OAM modes are expressed with the following equations [25]

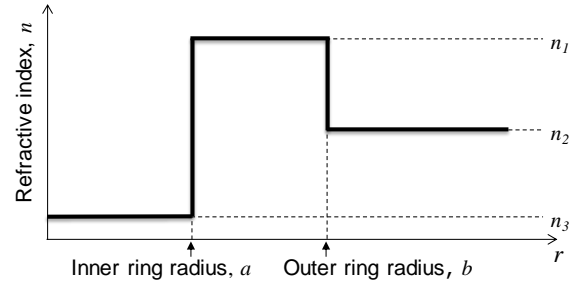


Fig. 1. Refractive index profile of a step-index RCF with depressed inner cladding.

$$OAM_{\pm l, m}^{\pm} = HE_{l+1, m}^{even} \pm jHE_{l+1, m}^{odd} \quad (1)$$

$$OAM_{\pm l, m}^{\mp} = EH_{l-1, m}^{even} \pm jEH_{l-1, m}^{odd} \quad (2)$$

where the sign in superscript denotes the direction of the circular polarization and the sign of l denotes the direction of the field rotation.

The direction of spin (i.e., polarization) and orbit (i.e., phase rotation) of the modes in an $OAM_{|l|,m}$ group can be either aligned or anti-aligned. Equations (1) and (2) represent the spin-orbit aligned and spin-orbit anti-aligned modes, respectively. These two types of modes become degenerate with small Δn_{eff} between HE and EH modes, and consequently, they would be strongly mixed resulting in an LP mode group, $LP_{l,m}$, having four-fold degeneracy. However, in the case where the Δn_{eff} is sufficiently increased, $OAM_{|l|,m}$ mode groups can be divided into two non-degenerate mode groups enabling the use of only 2×2 MIMO (to undo crosstalk within each of the spin-orbit aligned and anti-aligned OAM mode groups). A Δn_{eff} of 10^{-4} is usually considered to be necessary to mitigate significant mode coupling [35], but this requirement will vary depending on the target transmission configuration. It was experimentally reported that, with a Δn_{eff} of 10^{-4} , the modal crosstalk between OAM modes can be suppressed to less than -10 dB after >1-km long transmission [28].

Our goal is thus to find the RCF designs that support multiple OAM mode groups, $OAM_{|l|,m}$, whose Δn_{eff} are maximized under given geometric/functional constraints. It is important to note that all the guided OAM mode groups do not necessarily need to have large Δn_{eff} . Rather, we can rank the whole mode groups in accordance with their Δn_{eff} and then take only part of them for the data transmission. The number of mode groups chosen for the transmission is directly relevant to the increase of total data capacity. However, it is obvious that increasing Δn_{eff} becomes more challenging as the number of mode groups increases. In this paper, we will focus on designs optimized for MDM systems using three and four OAM mode groups (which corresponds to 12 and 16 information channels, respectively), and then discuss potential difficulties in further increasing the number of channels.

There are several important features that impact the suitability of an OAM mode for carrying data. OAM modes with radial order m larger than one are difficult to handle (i.e., signal generation and excitation) because of the complex modal distribution. Also, the OAM mode with $|l| = 1$ (which is composed of HE_{21} modes) is known to be inefficient for MDM

transmission due to the parasitic effects of the TE₀₁ and TM₀₁ modes [36]. This OAM mode is highly likely to experience a wide pulse spreading by two non-data-carrying modes having different propagation constant and consequently is not the best suited for low crosstalk transmission. While the (fundamental) OAM mode with $l = 0$ can be exploited for data transmission [14], the higher-order modes offer a richer target set with clear scalability advantages. For this reason, we will not target the fundamental mode in the optimization but will consider it a bonus when a design yields an exploitable $l = 0$ mode. In short, we will not consider $m > 1$, $l = 0$ nor $|l| = 1$ as data-carrying OAM mode groups in this paper.

We will evaluate all other OAM modes as targets, with suitability evaluated by three criteria. Firstly, the effective index separation from the closest neighboring mode must be sufficiently large. Next, modes should have acceptable bending loss over the entire wavelength range of interest. We will also consider the amount of deviation from perfect circular polarization of the target OAM modes (spin-orbit coupling [17-18]) because it is challenging to generate arbitrarily polarized (other than a linear or circular) vector modes. Hence, the final criterion reflects this concern, which we refer to as the polarization purity of the OAM mode.

Fig. 1 shows the refractive index profile of step-index RCF containing three parts: inner cladding, ring-shaped core, and outer cladding. We assume that the outer cladding is made of silica (SiO₂), i.e., $n_2 = 1.444$ at $1.55 \mu\text{m}$, and the core is made of silica doped with germanium dioxide (GeO₂). The inner cladding is assumed to be either air, i.e., $n_3 = 1$, or silica doped with fluorine (F). The outer cladding diameter is set to be standard $125 \mu\text{m}$. We use four parameters here, i.e., inner ring radius, a , outer ring radius, b , index contrast of core, $n_{0,\text{ring}} = n_1/n_2$, and index contrast of inner cladding, $n_{0,\text{iclad}} = n_3/n_2$, to find the optimum design using PSO algorithm.

III. PARTICLE SWARM OPTIMIZATION ALGORITHM

To initialize a swarm of particles, we first set the boundary

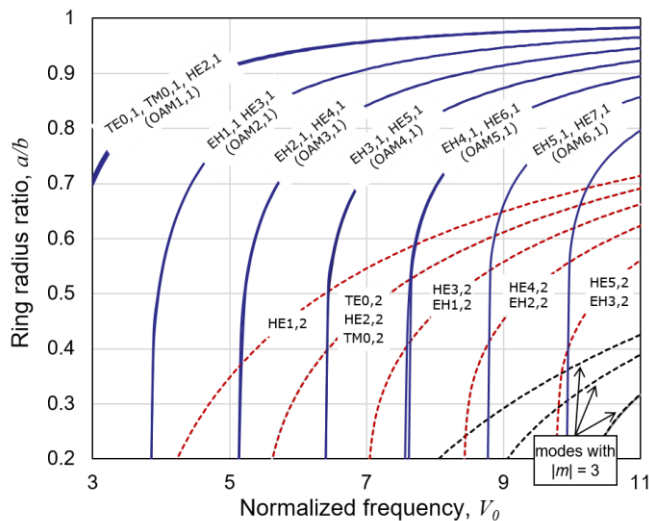


Fig. 2. Modal map defined by cutoff of the modes as a function of normalized frequency, V_0 , and ring radius ratio, a/b , with $n_1/n_2 = 1.021$ [37]. The modes labeled on each line become cutoff on the upper and left side of the line.

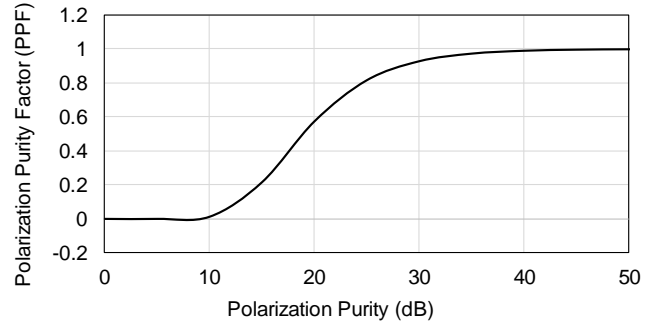


Fig. 3. The relationship between polarization purity factor and polarization purity in dB. The values of σ and w are set to 5 and 30, respectively.

for each parameter. Considering fabrication feasibility, we assumed $1.5 \mu\text{m} < a < 14 \mu\text{m}$, $4 \mu\text{m} < b < 16 \mu\text{m}$, $1.0021 < n_{0,\text{ring}} < 1.0276$, and $0.9654 < n_{0,\text{iclad}} < 1$. We define the normalized frequency as $V_0 = 2\pi b \lambda^{-1} \sqrt{n_1^2 - n_2^2}$, where λ is the wavelength. Since V_0 should be large enough to support at least three OAM mode groups (with $|l| \geq 2$), we conservatively assumed V_0 is larger than 5. From this requirement, assuming n_2 and λ are 1.444 and $1.53 \mu\text{m}$, respectively, we obtained a nonlinear boundary, $n_{0,\text{ring}}^2 > 1 + 0.7109 \times b^{-2}$. This nonlinear

constraint is based on the results obtained from an analytical study on vector modes in RCF, following the method in [37]. Fig. 2 shows the cutoff map of a step-index RCF as function of normalized frequency, V_0 , and ring radius ratio, a/b , with $n_{0,\text{ring}} = 1.021$ and $n_{0,\text{iclad}} = 1$. The ring radius ratio, a/b , was also set to be $0.3 < a/b < 0.95$ to avoid designs positioned in inappropriate regions of the cutoff map (e.g., too thin ring or an excessive number of guided modes with large radial order m).

To determine how well a particular design fits the optimal solution, we first need to be able to evaluate its modes. An ideal mode should meet the criteria (related to l , m , and bending loss) described in Section II and avoid severe crosstalk by maximizing Δn_{eff} and ensuring sufficient polarization purity. For the PSO algorithm, it is necessary to quantify all these factors. We define two parameters for this purpose: validity function $V(k)$ and polarization purity factor (PPF).

The $V(k)$ is an indicator function (zero/one) of the appropriateness of the mode as a data channel. Based on the discussion in Section II, $V(k)$ is set to zero if the eigenmode k has OAM with $m > 1$, $|l| = 0$ or $|l| = 1$. It is also set to zero when the bending loss is larger than 0.0001 dB/m at a bending radius of 30 mm at 1565 nm wavelength. Otherwise, $V(k)$ is set to one. This bending loss requirement is relevant to mode cutoff and it satisfies the criterion typically required for SMF [38]. The PPF is a value between 0 and 1 that represents the degree of circular polarization. This is defined in (3) with tuning factors σ and w , where $P_{\text{RCP}}(k)$ and $P_{\text{LCP}}(k)$ are the optical power of right circularly polarized portion and left circularly polarized portion, respectively, of an OAM mode based on eigenmode k .

$$\text{PPF}(k) = \left(1 - \exp\left(-\frac{|P_{\text{RCP}}(k) - P_{\text{LCP}}(k)| \text{ (dB)}}{\sigma} \right) \right)^w \quad (3)$$

As an example, the relationship between PPF and

polarization purity, $P_{\text{RCF}}/P_{\text{LCP}}$ (dB), is plotted in Fig. 3 for the case of $\sigma = 5$ and $w = 30$. The PPF varies roughly linearly with the polarization purity in the range of 10 dB to 30 dB, but saturates outside this range. We used these tuning values through our optimization process because in many cases the signal quality degradation becomes most important with crosstalk between -10 dB to -30 dB [39]. The bit-error rate (BER) penalty is known to be negligible when the crosstalk level is less than -30 dB for moderate quadrature-amplitude modulation (QAM) levels (<256), while -10 dB crosstalk causes unacceptable BER, even for quadrature phase-shift keying (QPSK). The tuning factors σ and w can be changed depending on the acceptable level of polarization purity.

We can now formulate a figure of merit to evaluate to what extent an eigenmode k is suitable for data transmission. We define a modal score $s(k)$ as follows

$$s(k) = \Delta n_{\text{eff}}(k) \times \text{PPF}(k) \times V(k) \quad (4)$$

Here, $\Delta n_{\text{eff}}(k)$ is the effective index difference of mode k with the nearest neighbor mode. As indicated by (4), the modal score of an eigenmode k increases with its Δn_{eff} and polarization purity unless the eigenmode has unacceptable features to be a data channel (i.e., $V(k) = 0$). It should be noted that each eigenmode of a particular design has its own modal score. Hence, we need another score, i.e., objective score, that represents the fitness of the overall fiber design.

Our optimization goal is to find the design that supports a given number of eigenmodes (or OAM mode groups) whose modal scores are maximized. For example, if we need three OAM mode groups (each derived from distinct pairs of eigenmodes) for data transmission, it is necessary to maximize the modal scores of six eigenmodes. Since the modal scores of all these modes should be as high as possible, we focus our attention on the sixth largest modal score as the objective score in this case. If we denote the n^{th} largest value of a set $\{S\}$ with

	b (μm)	a (μm)	n_1	n_3
All-glass	9.912	4.767	1.484	1.407
Hollow-core	10.001	4.508	1.484	1.000

cardinality k by $n\text{-max}_k \{S\}$, the objective function is defined as follows

$$F_n = n\text{-max}_k \{ \Delta n_{\text{eff}}(k) \times \text{PPF}(k) \times V(k) \} = n\text{-max}_k s(k) \quad (5)$$

where n is the target number of eigenmodes for data transmission.

We first generate 40 initial random design samples (i.e., particles) for the PSO algorithm. The objective score of each particle is evaluated at wavelengths of 1530 nm and 1565 nm, the shortest and the longest wavelength of the C-band, respectively. To ensure that the solution is appropriate over the whole C-band, we consider the worse objective score from these two extreme wavelengths. Each particle updates its position at the next iteration based on its current movement, the best position explored so far, and the global best position the swarm has explored. This process is iterated up to 200 times. We used the finite element method (FEM) to obtain the modal characteristics of each guiding mode at each iteration and at each particle. The values of inertia weight, cognitive attraction coefficient, and social attraction coefficient were 0.9, 0.5, and 1.25, respectively. Using these parameters, we were able to repeatedly obtain an optimal set of converged solutions within 50~100 iterations.

IV. RCF DESIGN OPTIMIZED FOR THREE OAM MODE GROUPS

RCFs can be cast into two groups depending on the existence of higher-order radial modes. In general, the higher-order radial modes (i.e., $m > 1$) propagate as guided modes when the ring radius ratio, a/b , is below a certain level. As discussed in

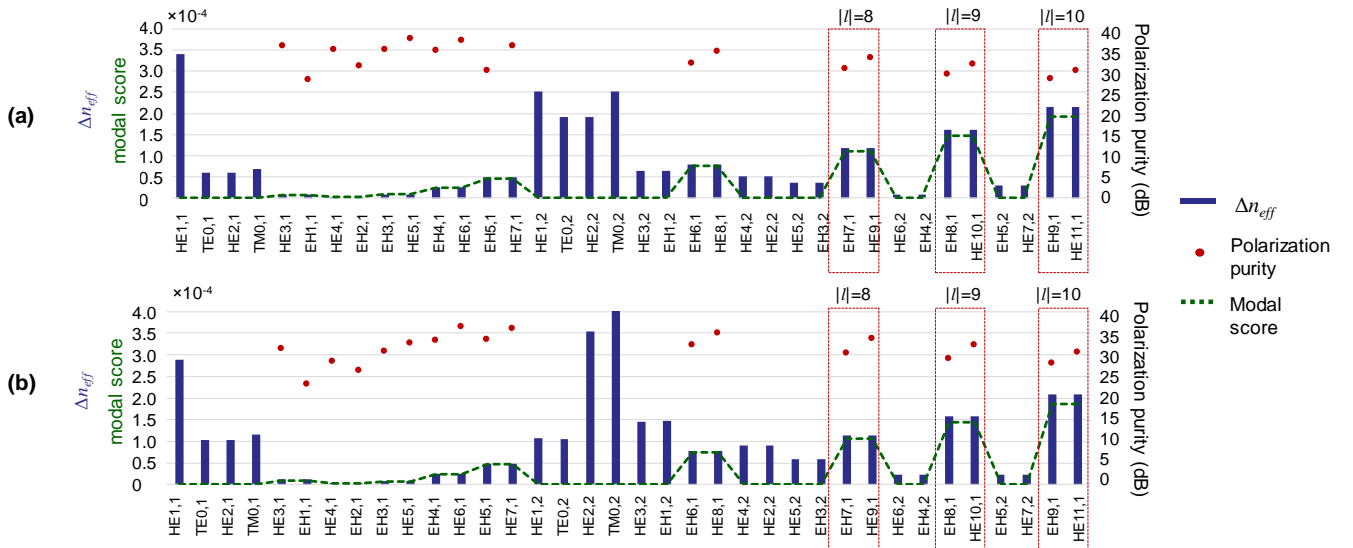


Fig. 4. For fiber design optimization allowing $m > 1$, the supported modes are shown along x-axis with their Δn_{eff} (left y-axis, blue bars), polarization purity (right y-axis, red dots), and modal score (left y-axis, green dashed line) for (a) all-glass RCF and (b) hollow-core RCF. Dashed red blocks show the three OAM mode groups with the largest modal score for each RCF.

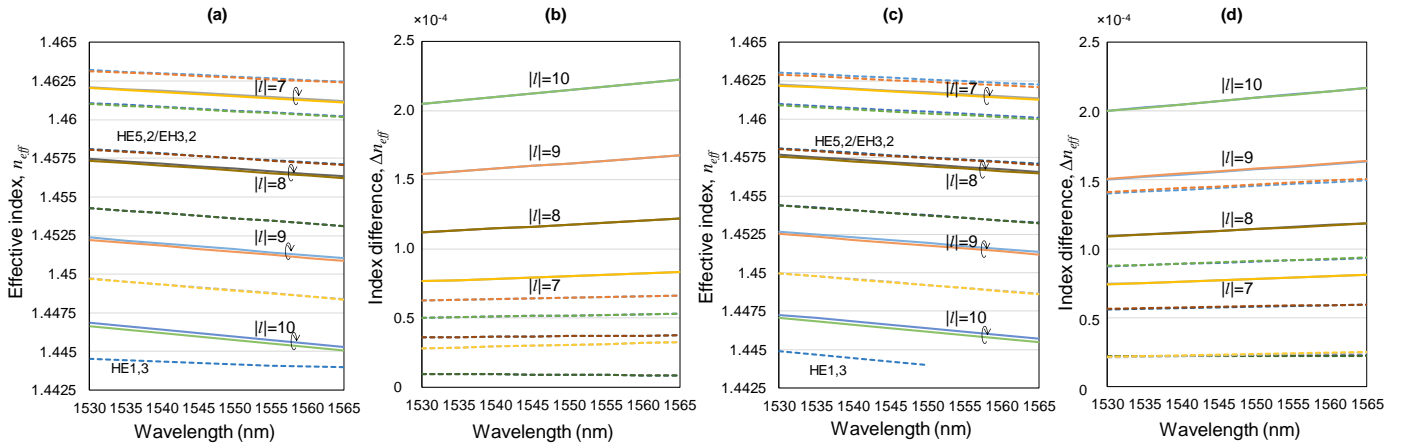


Fig. 5. Wavelength dependence over the C-band of: effective indices, n_{eff} , per mode for (a) all-glass RCF and (c) hollow-core RCF; and effective index differences, Δn_{eff} , for (b) all-glass RCF and (d) hollow-core RCF. Dashed lines correspond to untargeted modes, i.e., $m > 1$.

Section III, Fig. 2 plots the cutoff equations for OAM modes as a function of ring radius ratio and normalized frequency. As the ring radius ratio becomes larger, the ring becomes relatively thinner and modes start to cut off. Thinner rings with high ring radius ratios support only modes with $m=1$ (solid curves), while thicker rings can guide multiple ring modes (dashed curves) as well. One objective of this paper is to compare design choices in the thick vs. thin ring regimes. Despite the fact that the higher-order radial modes of thick-ring RCF are useless or even detrimental for data transmission, a thick-ring RCF provides a greater optimization space and potentially better solutions in the design space. The caveat remains that such solutions will risk having the higher-order radial modes act as parasitic modes: possible power leakage and/or pulse broadening due to undesired mode coupling [36]. In this section, we present the optimized designs obtained by the PSO algorithm for each case separately. We target three OAM mode groups for MDM data channels, and optimize fiber designs vis-à-vis our three criteria. We confirmed that these optimized designs have better objective scores than previously reported RCFs, validating our

optimization method using the PSO algorithm (Appendix).

A. RCF with higher-order radial modes (Thick-ring RCF)

The results of the PSO optimization are given in Table I for two RCF configurations: all glass RCF and hollow-core RCF. We specify b , a , n_1 , and n_3 , where n_1 and n_3 are specified at the wavelength of 1550 nm. For the optimization of hollow-core RCF using PSO, we used a fixed value of 1 for n_3 . Regardless of whether the inner cladding is air or glass, the two optimized designs have almost identical ring geometry, with the all-glass RCF having slightly smaller ring thickness. Fig. 4 shows all guided modes supported by each fiber with their Δn_{eff} with respect to the nearest mode, polarization purity, and modal score, at the wavelength of 1550 nm. Note that the polarization purity was calculated only for targeted, single-ring modes. We noticed a significant number of higher-order radial modes with $m=2$ for both fibers, all of which have modal score of zero (i.e., not targeted). Since our goal is to find the three OAM mode groups that are most suitable for data transmission, we chose the six eigenmodes with the best modal scores. As highlighted in the dashed blocks in Fig. 4, the OAM modes with $|l|=8, 9$,

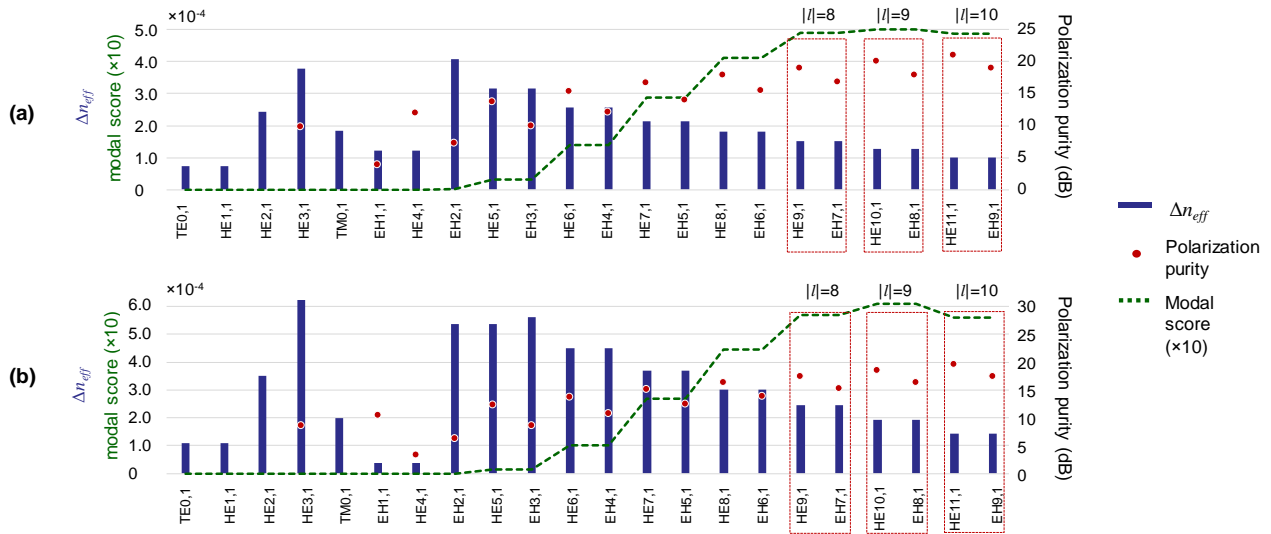


Fig. 6. For fiber design optimization allowing only $m = 1$, the supported modes are shown along x-axis with their Δn_{eff} (left y-axis, blue bars), polarization purity (right y-axis, red dots), and modal score ($\times 10$ magnified, left y-axis, green dashed line) for (a) all-glass RCF and (b) hollow-core RCF. Dashed red blocks show the three OAM mode groups with the largest modal score for each RCF.

TABLE II

OPTIMIZED VALUES OF THIN-RING RCFs FOR THREE OAM MODE GROUPS

	b (μm)	a (μm)	n_1	n_3
All-glass	13.249	11.718	1.484	1.394
Hollow-core	11.662	9.509	1.484	1.000

and 10 (i.e., OAM_{8,1}, OAM_{9,1}, and OAM_{10,1}) have the highest modal score for both all-glass and hollow-core RCF cases. The minimum Δn_{eff} and polarization purity of these modes were 1.18×10^{-4} and 28 dB for all-glass RCF, and 1.14×10^{-4} and 28 dB for hollow-core RCF, respectively, showing similar modal characteristics.

We also evaluated the wavelength dependency of n_{eff} and Δn_{eff} for both designs. Fig. 5(a) shows n_{eff} of the guiding modes as a function of wavelength for all-glass RCF. The solid lines indicate n_{eff} of OAM modes with $m=1$ while the dashed lines represent the values of neighboring higher-order radial modes. The n_{eff} matching between desired OAM modes and parasitic higher-order radial modes, which leads to phase matching and in turn severe mode coupling, was not observed over entire C-band. However, some separations between pairs of higher-order radial modes and OAM modes were small. For example, Δn_{eff} between EH₃₂ mode and EH₇₁ mode (which corresponds to OAM_{8,1} modes) was only 6.0×10^{-4} at 1530 nm. Although this value is 5 times larger than Δn_{eff} between two eigenmodes of OAM_{8,1} modes, it may become critical with deviation from the specified refractive index profile. Moreover, this structural error can also be crucial to modes near the cutoff condition. It is important to note that n_{eff} of the OAM_{10,1} modes is close to the cutoff boundary, making them vulnerable to unintended weakness in confinement (such as insufficient core doping or narrow ring thickness). We will discuss the impact of these types of fabrication error in Section VI.

Fig. 5(b) shows Δn_{eff} of the modes shown in Fig. 5(a) as a function of wavelength for all-glass RCF. The OAM_{8,1}, OAM_{9,1}, and OAM_{10,1} modes are shown to have Δn_{eff} larger than 10^{-4} over the C-band. The minimum Δn_{eff} of was calculated to be 1.13×10^{-4} at 1530 nm (for OAM_{8,1} mode).

Fig. 5(c) and (d) are the results for hollow-core RCF, and their tendency and values are very similar to the results obtained with all-glass RCF. This indicates that the utility of hollow-core for

lifting degeneracy of OAM modes is marginalized in this thick-ring case. We attribute this result to weak field intensity at the interface between core and inner cladding due to their small ring radius ratio, a/b , of ~ 0.45 .

B. RCF without higher-order radial modes (Thin-ring RCF)

To optimize RCFs with no higher-order radial modes allowed, we added a functional constraint to PSO algorithm: if any of guiding modes has the value of m larger than 1, the objective score is set to be zero regardless of the modal scores of targeted, single-ring modes. (Note that the objective score was the sixth largest modal score in Sec. IV.A.) Table II shows the optimized designs for all-glass and hollow-core RCFs. Compared to the optimum designs of thick-ring RCF, the designs shown in Table II had substantially thinner rings (higher ring radius ratio), as expected. Fig. 6 illustrates the mode contents of these RCFs with their Δn_{eff} , polarization purity, and modal score, at the wavelength of 1550 nm. For both designs, EH₂₁ modes (composing OAM_{3,1} modes) had a large Δn_{eff} which then gradually decreases as the order of modes increases. However, lower order modes tend to have low polarization purity resulting in serious degradation of the modal score. This problem became more critical for EH modes than for HE modes. For example, EH modes of OAM modes group with $|l| < 7$ had polarization purity worse than 15 dB for which the value of PPF (shown in eq. (4)) was only ~ 0.2 . This directly links to modal crosstalk and limits the number of usable modes because, upon demultiplexing, this component of EH _{$|l|-1$} will not belong to OAM _{$|l|$} mode but rather to OAM _{$|l|\pm 2$} mode, thereby introducing crosstalk. The three OAM mode groups having the largest modal score were OAM_{8,1}, OAM_{9,1}, and OAM_{10,1} for both RCFs. Nonetheless, their modal scores were only on the order of 0.50×10^{-4} , substantially lower than the values obtained for the thick-ring RCFs.

Fig. 7(a)-(b) and Fig. 7(c)-(d) show the wavelength dependency of n_{eff} and Δn_{eff} for all-glass RCF and for hollow-core RCF, respectively. Only the modes of interest are depicted, and the polarization purity for OAM_{8,1}, OAM_{9,1}, and OAM_{10,1} are also specified in Fig. 7(b) and (d). It should be noted that the polarization purity remained almost unchanged over the C-

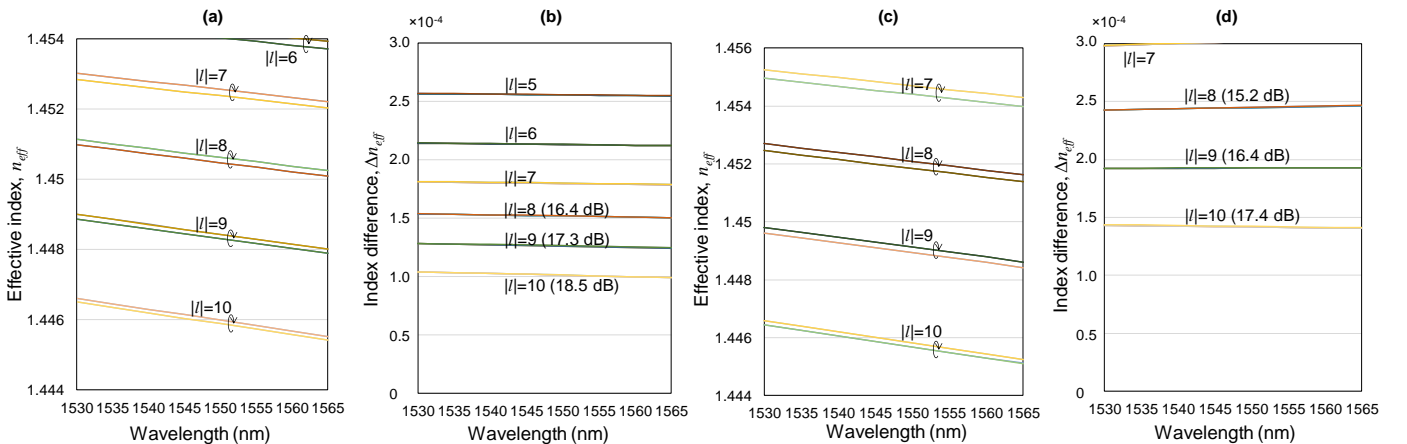


Fig. 7. Wavelength dependence over the C-band of: effective indices, n_{eff} , per mode for (a) all-glass RCF and (c) hollow-core RCF; and effective index differences, Δn_{eff} , for (b) all-glass RCF and (d) hollow-core RCF.

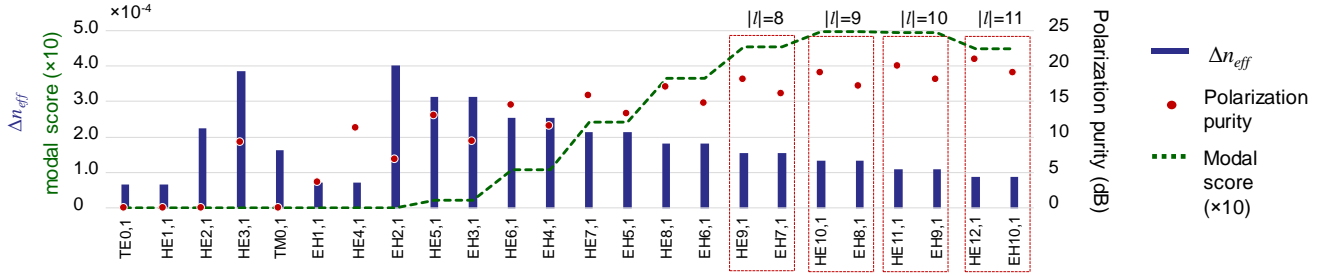


Fig. 8. For fiber design optimization allowing only $m = 1$, the supported modes are shown along x-axis with their Δn_{eff} (left y-axis, blue bars), polarization purity (right y-axis, red dots), and modal score ($\times 10$ magnified, left y-axis, green dashed line) for all-glass RCF. Dashed red blocks show the four OAM mode groups with the largest modal score.

TABLE III

OPTIMIZED VALUES OF ALL-GLASS RCF FOR FOUR OAM MODE GROUPS				
	b (μm)	a (μm)	n_1	n_3
Thick-ring	9.921	4.636	1.484	1.415
Thin-ring	13.965	12.354	1.484	1.395

band. Among OAM_{8,1}, OAM_{9,1}, and OAM_{10,1} modes, OAM_{8,1} had the largest Δn_{eff} while it was shown to have the worst polarization purity. The minimum Δn_{eff} and polarization purity of these modes at the entire C-band are 0.92×10^{-4} and 16.4 dB for all-glass RCF, and 1.41×10^{-4} and 15.2 dB for hollow-core RCF, respectively. These results indicate that the use of hollow-core helped increase the minimum Δn_{eff} by $\sim 53\%$ at the expense of polarization purity degradation of ~ 1.1 dB. Although, in contrast to thick-ring RCF, a hollow-core was beneficial in increasing Δn_{eff} for thin-ring RCF, we observed that this trade-off elicits an improvement of only $\sim 17\%$ in the modal scores. (The modal score of OAM_{10,1} for all-glass RCF is 4.8×10^{-5} , while the value is 5.6×10^{-5} for hollow-core RCF.) It is worth to note that these results are derived from the assumption the circularly polarized states are highly desirable for ease of multiplexing/demultiplexing. If we consider excitation of non-uniform elliptically polarized modes into the fiber using q-plates [27], for example, the utility of using a hollow-core could be enhanced.

V. OPTIMIZED RCF DESIGNS FOR FOUR OAM MODE GROUPS

The PSO algorithm can also be used to find RCF designs optimized for MDM systems employing a higher number of

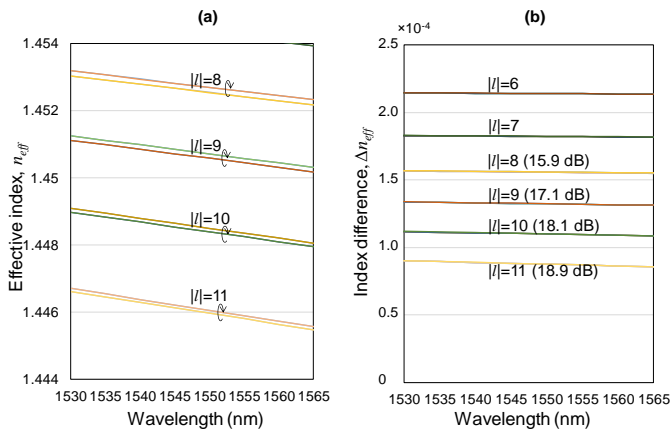


Fig. 9. Wavelength dependence over the C-band of (a) the effective indices, n_{eff} , and (b) the effective index differences, Δn_{eff} , of each mode of an all-glass RCF supporting four OAM mode groups.

OAM channels. Table III reports the all-glass RCF designs optimized for four OAM mode groups. In the case of the RCF with a thick ring, the design was very similar to the one obtained for three OAM mode groups (Table I), indicating that this design is close to optimum for both cases. We can thus simply increase the number of channels by using one of the unused OAM modes of the RCF. As it can be seen in Fig. 5(b), OAM_{7,1} modes were shown to have the minimum Δn_{eff} of 0.77×10^{-4} over entire C-band, which is an acceptable level for data transmission over length of < 1 km [28]. This value was increased to 0.83×10^{-4} for the design described in Table III. The n_{eff} of OAM_{7,1} modes, however, are close to those of HE₄₂ and EH₁₂, as shown in Fig. 5(a). This poses a potential risk of undesirable mode coupling in the presence of geometric perturbation.

The design of thin-ring RCF optimized for four OAM mode groups is also described in Table III. Fig. 8 shows various modal characteristics of its guided modes at the wavelength of 1550 nm. Compared to the design for three OAM mode groups (shown in Fig. 6(a)), OAM_{11,1} modes become the additional guided modes at the expense of slightly reduced scores of OAM_{8,1} modes. Consequently, we were able to exploit four OAM mode groups, i.e., $|l|=8, 9, 10$, and 11, in accordance with the modal score, as shown in the dashed blocks. The wavelength dependencies of n_{eff} and Δn_{eff} were also evaluated and the results are shown in Fig. 9. All four OAM mode groups had Δn_{eff} and polarization purity larger than 0.86×10^{-4} and 15.9 dB, respectively, over the C-band.

From the results above, we notice that the designs optimized for four OAM modes groups do not have remarkable differences from the designs for three OAM mode groups. This fact indicates that we do not have much room to improve the RCF design in order to increase the number of OAM modes while maintaining high Δn_{eff} and polarization purity simultaneously (i.e., high objective score). Considering that the values of Δn_{eff} and polarization purity obtained above would barely meet the practical requirement, increasing the number of OAM mode groups beyond four with this type of step-index RCF will be challenging.

VI. DESIGN TOLERANCE AND DISCUSSIONS

Structural inaccuracies of an optical fiber are inevitable in the fabrication process. Therefore, tolerance analysis is especially important for designs derived by PSO algorithm where the global best solution is found without any consideration for

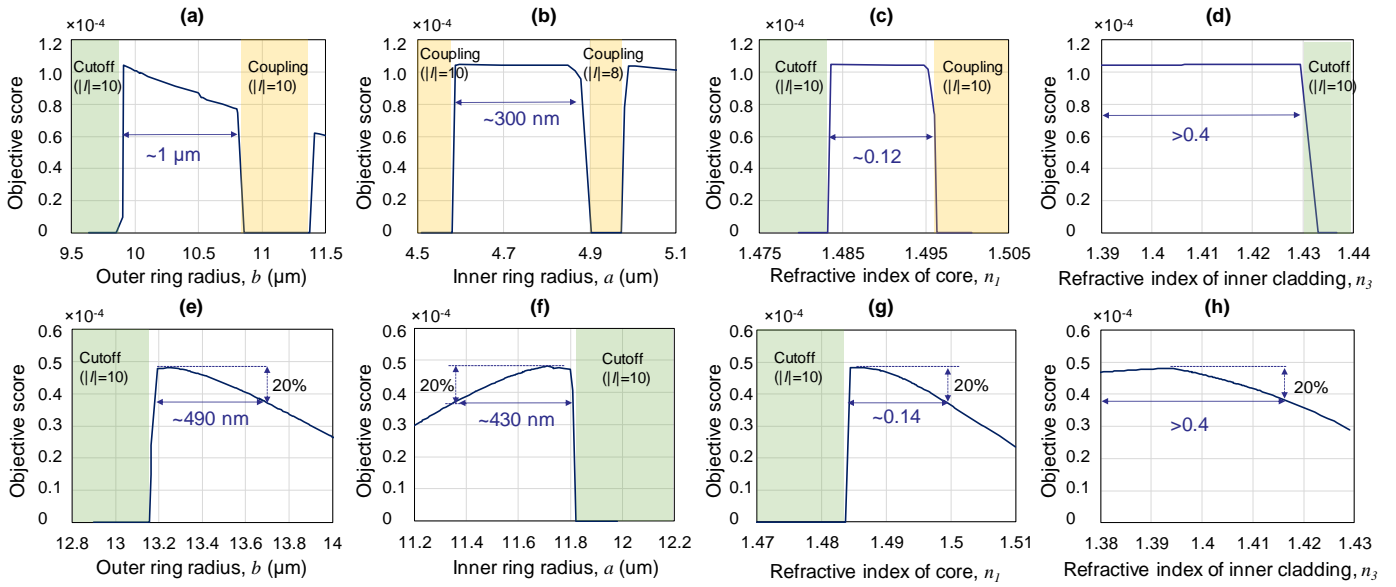


Fig. 10. The variations of objective score obtained as we change the value of: (a) b , (b) a , (c) n_1 , and (d) n_3 , of the optimized thick-ring all-glass RCF; and (e) b , (f) a , (g) n_1 , and (h) n_3 of the optimized thin-ring all-glass RCF. Each RCF was optimized for the use of three OAM mode groups.

design margin. Fig. 10 shows the impact of the variation of a single parameter on the objective score, while holding other parameters fixed. Fig. 10(a)-(d) show the results for all-glass RCF with a thick ring (derived in Section IV.A, Table I). The results for hollow-core RCF are not shown here as they are similar to that of all-glass RCF. The structural deviations mainly caused two problems: the mode coupling between neighboring modes and the cutoff of the highest mode. As can be seen in Fig. 10(d), for instance, excessively high n_3 (above 1.43) relaxed mode confinements and made the $\text{OAM}_{10,1}$ mode cutoff, resulting in the objective score of zero. The same cutoff appeared when the n_1 decreased lower than 1.484, as shown in Fig. 10(c). In the case that n_1 became higher than 1.495, $\text{OAM}_{10,1}$ modes started to couple with the HE_{31} mode, which is

closely packed in terms of n_{eff} . Nevertheless, the sensitivity of objective scores to refractive index, n_1 or n_3 , was negligibly small over a wide range of index variation (e.g., ~ 0.12 for n_1), large enough to control in fabrication.

The objective score was relatively more sensitive to small variation of ring radii than that of refractive indices, especially for b . More importantly, due to the unwanted coupling with peripheral higher-order radial modes, the margin of inner ring radius, a , was found to be only ~ 300 nm. This issue became more problematic when we attempted to increase the number of OAM mode groups for data transmission. Performing the same analysis for the all-glass RCF optimized for four OAM groups (derived in Section V), the margin shrunk drastically to ~ 170 nm for b , as shown in Fig. 11(a). This is because of the mode coupling between $\text{OAM}_{7,1}$ modes and the higher-order radial modes such as HE_{42} .

Fig. 10(e)-(h) show the change of objective scores caused by the variation of each parameter for the all-glass RCF having a thin-ring (derived in Section IV.B). As opposed to the thick-ring RCF, due to the absence of parasitic modes, there was no prohibited area where serious mode couplings may occur. However, the objective scores for thin-ring RCF were more sensitive to small variations of the design compared to the case of thick-ring RCF. For instance, the objective score of $\sim 0.48 \times 10^{-4}$ obtainable at $b = 13.25 \mu\text{m}$ was decreased to 0.40×10^{-4} by a deviation of only ~ 360 nm. If we assume that 20% of decrease from a peak is acceptable, the margin would be 490 nm, and 430 nm for b and a , respectively. Contrary to our expectation, the margins for thin-ring RCF were not significantly increased compared to the case of thick-ring RCF aiming at the same number of OAM channels. This is because, for thin-ring RCF, the mode intensity at the interface between core and cladding, which plays an important role in determining the Δn_{eff} , decreases rapidly even with a small change of the ring thickness [21]. However, an advantage of using thin-ring RCF was that the design margins were stable even for the higher

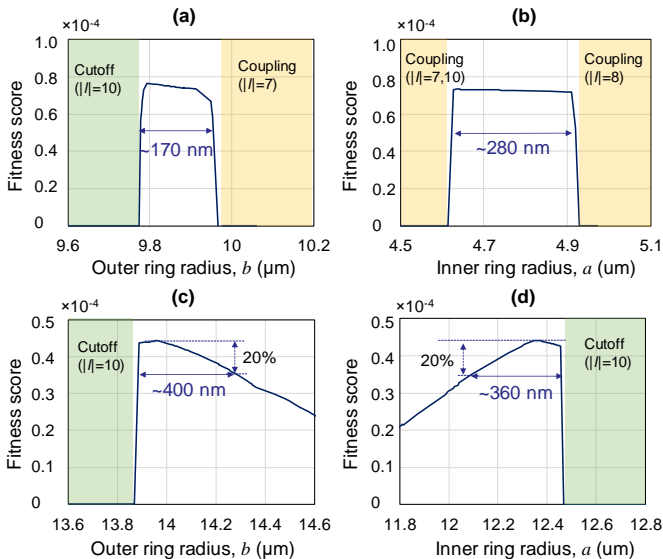


Fig. 11. The variations of objective score obtained as we change the value of: (a) b and (b) a of the optimized thick-ring all-glass RCF; and (c) b and (d) a of the optimized thin-ring all-glass RCF. Each RCF was optimized for the use of four OAM mode groups.

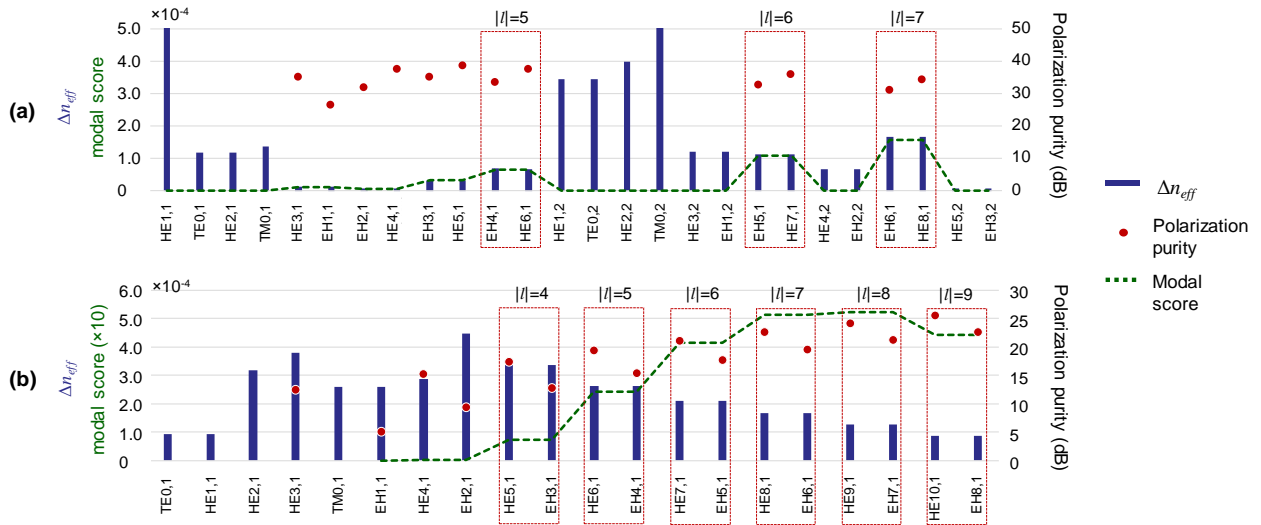


Fig. 12. For previously published fiber designs, the supported modes are shown along x-axis with their Δn_{eff} (left y-axis, blue bars), polarization purity (right y-axis, red dots), and modal score (left y-axis, green dashed line) for (a) a thick-ring RCF [29] and (b) a thin-ring RCF [27] (both shown in Table IV). Dashed red blocks show the modes that were used for transmission experiments.

number of OAM mode groups. Fig. 11(c)-(d) shows the impact of structural deviation on objective score for thin-ring RCF optimized for four OAM mode groups (derived in Section V). The margins of b and a were found to be 400 nm and 360 nm, respectively, assuming the 20% of decrease from a peak is acceptable.

According to the results above, the thick-ring RCF is generally more suitable to achieve higher score than the thin-ring RCF if the fabrication error can be strictly controlled. If we cannot guarantee the accuracy of ring radii to a margin of around ± 100 nm, we expect the thin-ring RCF will be favorable in terms of fabrication, especially for a higher number of OAM mode groups.

VII. CONCLUSION

We have studied the design of step-index RCFs with depressed inner cladding for MDM optical transmission system using OAM modes. In order to find the ideal design concept, we analyzed four different categories of RCFs: all-glass RCFs with a thick or thin ring, and hollow-core RCF with a thick or thin ring. For each category, we found an optimum design that satisfies our criteria by using a PSO algorithm. The objective function was defined to quantify the performance of each candidate design by considering the minimum Δn_{eff} and

	b (μm)	a (μm)	n_1	n_2
Thick-ring [29]	8.25	3.05	1.479	1.000
Thin-ring [27]	11.70	9.40	1.479	1.000

polarization purity of the desired OAM mode groups, which are strongly related to the amount of modal crosstalk in MDM systems. We confirmed that the PSO algorithm can effectively optimize fiber design to meet many different requirements. We expect the effectiveness of this method to increase as the number of design parameters increases with more complex fibers (beyond step index). Based on the optimized designs, we first investigated the impact of using a hollow-core RCF versus an all-glass RCF. The results showed that the use of a hollow-core has a negligible effect on increasing Δn_{eff} or polarization purity of thick-ring RCF. One can expect increase of Δn_{eff} for thin-ring RCF, while the sacrifice of polarization purity is inevitable. Considering the fact that hollow-core RCF involves more complex fabrication, and is more mechanically vulnerable than all-glass RCF, the practical advantage of using a hollow-core is highly dependent on the techniques available to circumvent the polarization purity degradation of hollow-core RCF, e.g., q-plate [27]).

We compared the design concepts with regard to their ring

TABLE V
COMPARISON OF MODAL CHARACTERISTICS AND SCORES BETWEEN DIFFERENT HOLLOW-CORE RCF DESIGNS

	BU Thick-ring [29]			Thick-ring (Sec. IV.A)			BU Thin-ring [27]			Thin-ring (Sec. IV.B)		
	5	6	7	8	9	10	7	8	9	8	9	10
Topological charge $ l $												
$\Delta n_{eff} (\times 10^{-4})$	0.65	1.07	1.60	1.09	1.50	1.98	1.64	1.26	0.88	2.42	1.92	1.44
Polarization purity (dB)	33.4	32.4	31.0	30.36	29.07	28.1	16.3	17.7	18.9	15.2	16.4	17.4
Modal score ($\times 10^{-4}$)	0.62	1.02	1.50	1.01	1.37	1.78	0.51	0.52	0.45	0.56	0.61	0.56
Objective score ($\times 10^{-4}$)	0.62			1.01			0.45			0.56		

thicknesses. Higher objective scores were obtained with thick-ring RCF because thin-ring RCF generally induced low polarization purity. When we targeted three OAM mode groups as data channels, the optimum designs of thick-ring all-glass RCF showed minimum Δn_{eff} of 1.18×10^{-4} and 28.0 dB polarization purity over the C-band, whereas the values of only 0.92×10^{-4} and 16.4 dB were achievable for thin-ring all-glass RCF. However, thick-ring RCF is extremely sensitive to fabrication error of ring dimension because of undesirable mode coupling between desired modes and unwanted higher-order radial modes. Therefore, the thick-ring RCF is advantageous only if the fabrication error can be strictly managed. We also found that it would be difficult to increase the number of spatial channels more than 16 (i.e., four OAM mode groups), while keeping Δn_{eff} and polarization purity reasonably high.

APPENDIX

To validate the effectiveness of our objective function and PSO algorithm, we compared the RCF designs optimized by PSO algorithm with the designs that have been reported previously in the literature. More precisely, we investigate two hollow-core RCFs. The first design was used to demonstrate an MDM transmission over 12 OAM modes (i.e., 3 OAM mode groups) [29]. Although this fiber supports several higher-order radial modes, the OAM_{|l|,1} modes with $|l|=5, 6, \text{ and } 7$ were successfully exploited for data transmission. Thus, it can be categorized as a thick-ring RCF. In [27], a thin-ring hollow-core RCF was also proposed to realize a higher number of spatial channels. Table IV shows the structural values of these two designs from Boston University (BU) that we used for comparison. We approximated their measured profiles by step-index profiles to obtain these values; our comparison should be made under the same geometrical and conditional constraints to evaluate the effectiveness of PSO algorithm. We first numerically evaluated the modal characteristics for these hollow-core RCFs, and then calculated the modal scores by using the objective function we defined in Sec. III. The Δn_{eff} , polarization purity, and modal score of each guided mode are described in Fig. 12. The dashed blocks in Fig. 12 indicates the modes with low crosstalk that were actually used for experimental demonstration [27,29]. Despite the fact that our design strategy is aiming for the generation of circularly polarized OAM modes in contrast to the approach used in [27], these selected modes coincide with the modes having the highest modal scores. It clearly implies that our objective function is a reasonable measure of modal quality as a channel for MDM transmission.

Next, we compared the designs shown in Table IV with our designs optimized by PSO algorithm in Section IV (which are aiming for the use of three OAM mode groups). For comparison, we chose only three OAM mode groups with the highest modal scores. Table V reports the modal characteristics and modal scores of the three OAM mode groups supported by each design as well as its objective score. The results show that, for both thick and thin-ring RCF, PSO-optimized designs have higher objective scores than the designs in Table IV. This result

validates that PSO algorithm can become a simple and effective tool to find an optimum solution for RCF design.

ACKNOWLEDGMENT

The authors thank Dr. Haisu Li for insightful discussions.

REFERENCES

- [1] D. J. Richardson, J. M. Fini, and L. E. Nelson, "Space-division multiplexing in optical fibres," *Nature Photon.*, vol. 7, pp. 354–362, 2013.
- [2] A. Al Amni, A. Li, S. Chen, X. Chen, G. Gao, and W. Shieh, "Dual-LP₁₁ mode 4×4 MIMO-OFDM transmission over a two-mode fiber," *Opt. Express*, vol. 19, no. 17, pp. 16672–16678, 2011.
- [3] S. Randel, R. Ryf, A. Sierra, P. Winzer, A. H. Gnuack, C. Bolle, R.-J. Essiambre, D. W. Peckham, A. McCurdy, and R. Lingle, "6 × 56-Gb/s mode-division multiplexed transmission over 33-km few-mode fiber enabled by 6×6 MIMO equalization," *Opt. Express*, vol. 19, no. 17, pp. 16697–16707, 2011.
- [4] N. Bai, E. Ip, Y.-K. Huang, E. Mateo, F. Yaman, M.-J. Li, S. Bickham, S. Ten, J. Linares, C. Montero, V. Moreno, X. Prieto, V. Tse, K. M. Chung, A. P. T. Lau, H.-Y. Tam, C. Lu, Y. Luo, G.-D. Peng, G. Li, and T. Wang, "Mode-division multiplexed transmission with inline few-mode fiber amplifier," *Opt. Express*, vol. 20, no. 3, pp.2668–2680, 2012.
- [5] J. van Weerdenburg, A. V. Benitez, R. van Uden, P. Sillard, D. Molin, A. Amezcua-Correa, E. Antonio Lopez, M. Kuschnerov, F. Huijskens, H. de Waardt, T. Koonen, R. Amezcua-Correa, and C. Okonkwo, "10 spatial mode transmission using low differential mode delay 6-LP fiber using all-fiber photonic lanterns," *Opt. Express*, vol. 23, no. 19, pp. 24759–24769, 2015.
- [6] J. Van Weerdenburg, R. Ryf, J. C. Alvarado-Zacarias, R. A. Alvarez-Aguirre, N. K. Fontaine, H. Chen, R. Amezcua-Correa, T. Koonen, and C. Okonkwo, "138 Tbit/s transmission over 650 km graded index 6-mode fiber," in *Proc. 43rd Eur. Conf. Exhib. Opt. Commun.*, 2017, paper Th.PDP.A.4.
- [7] N. K. Fontaine, R. Ryf, H. Chen, A. V. Benitez, E. Antonio Lopez, R. Amezcua-Correa, B. Guan, B. Ercan, R. Scott, S. J. B. Yoo, L. E. Grüner-Nielsen, Y. Sun, and R. Lingle, "30×30 MIMO transmission over 15 spatial modes," in *Proc. Opt. Fiber Commun. Conf.*, 2015, paper Th5C.1.D.
- [8] R. Ryf, N. K. Fontaine, H. Chen, B. Guan, S. Randel, N. Sauer, S. J. B. Yoo, A. Koonen, R. Delbue, P. Pupalakis, A. Sureka, R. Shubochkin, Y. Sun, and R. Lingle, "23 Tbit/s transmission over 17-km conventional 50 μm graded-index multimode fiber," in *Proc. Opt. Fiber Commun. Conf.*, 2014, paper Th5B.1.
- [9] D. Soma, Y. Wakayama, K. Igarashi, and T. Tsuritani, "Partial MIMO-based 10-mode-multiplexed transmission over 81 km weakly-coupled few-mode fiber," in *Proc. Opt. Fiber Commun. Conf.*, 2017, paper M2D.4.
- [10] N. Bozinovic, Y. Yue, Y. Ren, M. Tur, P. Kristensen, H. Huang, A. E. Willner, and S. Ramachandran, "Terabit-scale orbital angular momentum mode division multiplexing in fibers," *Science*, vol. 340, pp. 1545–1548, 2013.
- [11] H. Huang, G. Milione, M. P. J. Lavery, G. Xie, Y. Ren, Y. Cao, N. Ahmed, T. A. Nguyen, D. A. Nolan, M.-J. Li, M. Tur, R. R. Alfano, and A. E. Willner, "Mode division multiplexing using an orbital angular momentum mode sorter and MIMO-DSP over a graded-index few-mode optical fibre," *Sci. Rep.*, vol. 5, no. 14931, 2015.
- [12] Y. Yue, Y. Yan, N. Ahmed, J.-Y. Yang, L. Zhang, Y. Ren, H. Huang, K. Birnbaum, B. Erkmen, S. Dolinar, M. Tur, and A. Willner, "Mode properties and propagation effects of optical orbital angular momentum (OAM) modes in a ring fiber," *IEEE Photon. J.*, vol. 4, no. 2, pp. 535–543, 2012.
- [13] P. Boffi, P. Martelli, A. Gatto, and M. Martinelli, "Mode-division multiplexing in fibre-optic communications based on orbital angular momentum," *J. Opt.*, vol. 15, no. 7, pp. 075403, 2013.
- [14] R. M. Nejad, K. Allahverdyan, P. Vaity, S. Amiralizadeh, C. Brunet, Y. Messaddeq, S. LaRochelle, and L. A. Rusch, "Mode division multiplexing using orbital angular momentum modes over 1.4-km ring core fiber," *J. Lightwave Technol.*, vol. 34, no. 18, pp. 4252–4258, 2016.
- [15] F. Feng, X. Jin, D. O'Brien, F. P. Payne, and T. D. Wilkinson, "Mode group multiplexed transmission using OAM modes over 1 km ring-core

- fiber without MIMO processing,” in *Proc. Opt. Fiber Commun. Conf.*, 2017, paper Th2A.43.
- [16] D. Andrews, “Structured light and its applications”, Academic Press, New York, 2008.
- [17] S. Ramachandran, P. Gregg, P. Kristensen, and S. E. Golowich, “On the scalability of ring fiber designs for OAM multiplexing,” *Opt. Express*, vol. 23, no. 3, pp. 3721–3730, 2015.
- [18] S. Golowich, “Asymptotic theory of strong spin-orbit coupling in optical fiber,” *Opt. Lett.*, vol. 39, no. 1, pp. 92–95, 2014.
- [19] C. Brunet, B. Ung, L. Wang, Y. Messaddeq, S. LaRochelle, and L. A. Rusch, “Design of a family of ring-core fibers for OAM transmission studies,” *Opt. Express*, vol. 23, no. 8, pp. 10553–10563, 2015.
- [20] G. Zhu, Z. Hu, X. Wu, C. Du, W. Luo, Y. Chen, X. Cai, J. Liu, J. Zhu, and S. Yu, “Scalable mode division multiplexed transmission over a 10-km ring-core fiber using high-order orbital angular momentum modes,” *Opt. Express*, vol. 26, no. 2, pp. 594–604, 2018.
- [21] B. Ung, P. Vaity, L. Wang, Y. Messaddeq, L. A. Rusch, and S. LaRochelle, “Few-mode fiber with inverse-parabolic graded-index profile for transmission of OAM-carrying modes,” *Opt. Express*, vol. 22, no. 15, pp. 18044–18055, 2014.
- [22] W. Tian, H. Zhang, X. Zhang, L. Xi, W. Zhang, and X. Tang, “A circular photonic crystal fiber supporting 26 OAM modes,” *Opt. Fiber Technol.*, vol. 30, pp. 184–189, 2016.
- [23] S.-H. Li and J. Wang, “A compact trench-assisted multi-orbital-angular momentum multi-ring fiber for ultrahigh-density space-division multiplexing (19 rings \times 22 modes),” *Sci. Rep.*, vol. 4, no. 3853, 2014.
- [24] S. Ramachandran and P. Kristensen, “Optical vortices in fiber,” *Nanophotonics*, vol. 2, no. 5–6, pp. 455–474, 2013.
- [25] C. Brunet, P. Vaity, Y. Messaddeq, S. LaRochelle, and L.A.Rusch, “Design, fabrication and validation of an OAM fiber supporting 36 states,” *Opt. Express*, vol. 22, no. 21, pp. 26117–26127, 2014.
- [26] P. Gregg, P. Kristensen, and S. Ramachandran, “Conservation of orbital angular momentum in air-core optical fibers,” *Optica*, vol. 2, no. 3, pp. 267–270, 2015.
- [27] P. Gregg, P. Kristensen, A. Rubano, S. Golowich, L. Marrucci, and S. Ramachandran, “Spin-orbit coupled, non-integer OAM fibers: Unlocking a new eigenbasis for transmitting 24 uncoupled modes,” in *Proc. Lasers Electro-Opt.*, 2016, Paper JTh4C.7.
- [28] P. Gregg, P. Kristensen, and S. Ramachandran, “13.4 km OAM state propagation by recirculating fiber loop,” *Opt. Express*, vol. 24, no. 17, pp. 18938–18947, 2016.
- [29] K. Ingerslev, P. Gregg, M. Galili, F. Da Ros, H. Hu, F. Bao, M. Usuga Castaneda, P. Kristensen, A. Rubano, L. Marrucci, K. Rottwitt, T. Morioka, S. Ramachandran, and L. Oxenløwe, “12 mode, WDM, MIMO-free orbital angular momentum transmission,” *Opt. Express*, vol. 26, no. 16, pp. 20225–20232, 2018.
- [30] R. C. Eberhart and Y. Shi, “Particle swarm optimization: developments, applications and resources,” in *Proc. Congr. Evolutionary Computation*, vol. 1, 2001.
- [31] R. Hassan, B. Cohanin, and O. de Weck, “A comparison of particle swarm optimization and the genetic algorithm,” in *Proc. AIAA/ASME/ASCE/AHS/ASC 46th Structures, Structural Dynamics and Materials Conf.*, 2005.
- [32] H. Li, G. Ren, Y. Gao, Y. Lian, M. Cao, and S. Jian, “Particle swarm optimization of single-mode trench-assisted bend-insensitive fibers,” *IEEE Photon. Technol. Lett.*, vol. 27, no. 2, pp. 1293–1296, 2015.
- [33] S. Baskar, R. T. Zheng, A. Alphones, N. Q. Ngo, and P. N. Suganthan, “Particle Swarm Optimization for the Design of Low-Dispersion Fiber Bragg Gratings,” *IEEE Photon. Technol. Lett.*, vol. 17, no. 3, pp. 615–617, 2005.
- [34] A. Mowla and N. Granpayeh, “Optimum design of a hybrid erbium-doped fiber amplifier/fiber Raman amplifier using particle swarm optimization,” *App. Optics*, vol. 48, no. 5, pp. 979–984, 2009.
- [35] A. Corsi, J. H. Chang, L. A. Rusch, and S. LaRochelle, “Design of highly elliptical core ten-mode fiber for space division multiplexing with 2 \times 2 MIMO,” *IEEE Photon. J.*, vol. 11, no. 2, pp. 1–10, 2019.
- [36] R. M. Nejad, L. Wang, J. Lin, S. LaRochelle, and L. A. Rusch, “The impact of modal interactions on receiver complexity in OAM fibers,” *J. Lightw. Technol.*, vol. 35, no. 21, pp. 4692–4699, 2017.
- [37] C. Brunet, B. Ung, P. A. Bélanger, Y. Messaddeq, S. LaRochelle, and L. A. Rusch, “Vector mode analysis of ring-core fibers: Design tools for spatial division multiplexing,” *J. Lightw. Technol.*, vol. 32, no. 23, pp. 4648–4659, 2014.
- [38] T. Matsui, K. Nakajima, and C. Fukai, “Applicability of photonic crystal fiber with uniform air-hole structure to high-speed and wide-band transmission over conventional telecommunication bands,” *J. Lightw. Technol.*, vol. 27, no. 23, pp. 5410–5416, 2009.
- [39] P. J. Winzer, A. H. Gnauck, A. Koncewiczowska, F. Jorge, and J.-Y. Dupuy, “Penalties from in-band crosstalk for advanced optical modulation formats,” in *Proc. Eur. Conf. Opt. Commun.*, 2011, Paper Tu.5.B.7.